Proceedings of the ASME 2010 3rd Joint US-European Fluids Engineering Summer Meeting and 8th International Conference on Nanochannels, Microchannels, and Minichannels
FEDSM-ICNMM2010
August 1-5, 2010, Montreal, Canada

FEDSM-ICNMM2010-30157

LARGE-EDDY SIMULATION OF URBAN FLOWS: POROUS-MEDIA ANALOGY

Andrzej A. Wyszogrodzki and Piotr K. Smolarkiewicz

National Center for Atmospheric Research
Boulder, Co, USA

ABSTRACT

In analogy to theoretical formulation for the microscopic fluid flows in porous media [1] we perform series of numerical simulations of urban boundary layer flows through realistic street-level building structures of the Oklahoma City downtown area. The corresponding numerical solutions relate the morphology of the real building structures to topological and geometrical properties of the physical media. We analyze the results in statistical terms of random porous media, seeking the relation between the momentum flux and the macroscopic pressure gradient; i.e., a high-Reynolds-number analogy of the Darcy's law. We relate urban ``pore-space'' spatial properties (e.g., homogeneity and anisotropy) to the estimates of permeability and tortuosity. We evaluate further the utility of a porous-media analogy for parameterizing urban effects in the mesoscale weather and air-quality prediction models.

INTRODUCTION

A typical representation of the dynamics of urban environments in a numerical models is based on computing the cumulative Stoke's drag from the aggregated morphological parameters of the urban canopy at the different scales (100 m – 10 km). Initially the different coarse resolution datasets (usually up to 1km resolution) were generated in the form of land use/land cover (LULC) data [2]. Beside the different classification approaches and small number of urban land use types, LULC datasets themselves have limitations. In particular, the urbanization data for cities experiencing massive growth can become rapidly outdated, because of the masked heterogeneity of morphological characteristics with aggregation of different building structures into a single category. The information about urban surface extent with a set of representative geometric, radiation, thermodynamic, and surface cover parameters is collected in nationwide urban footprint databases. Such databases are founded on information coming from traditional LULC datasets (USGS), nighttime satellite imagery (e.g. Landsat). More recently a detailed collection of the largest US metropolitan areas footprints was created at LANL using 2000 US Census and 1999 State Business Directory data [3].

A finer datasets of Urban Terrain Zones (UTZ) contain the properties of the Urban Canopy Layer (UCL) important for the micro-scale simulations: see [4], [5]. The UTZ classifications are based on detailed measures of the three-dimensional building and tree morphology, automated analysis of satellite data (e.g., synthetic aperture radar), and airborne lidar. A nationally consistent coverage for metropolitan areas includes information about building height, geometry, and density (e.g., mean building height, plan area density, frontal area density, sky view factor, street-canyon length and width) as well as information about street pattern, lot configuration, and type of constructions. The non-building morphology types include trees, shrubs, crops, grass, bare soil, water, marsh, and various types of impervious surfaces as highways, roads, streets, parking lots, and gathering spaces. The computed information uses geographic information system (GIS) and is packaged for use in typical mapping software (e.g., ArcGIS) for importation to modeling systems. A second generation National Building Statistics Database (NBSD2) consisting of gridded fields created at 250m and 1 km sizes for urban areas [6]. Recently National Urban Database and Access Portal Tool (NUDAPT) consist of detailed building and other urban morphological structures imagery information at pixel resolution of order 1 m are being acquired for 133 urban centers in the USA [7].

The information based on LULC and morphological-based aerodynamic characteristics (roughness length, displacement height, depth of roughness sub-layer or conductance) have served for many years to define surface parameters in the whole extent of mesoscale meteorological and dispersion models domain. Here we attempt to: i) characterize complex urban geometries in terms of pore space properties such as heterogeneity and anisotropy of porosity, permeability and tortuosity; and evaluate the usability of such a characterization in mesoscale modeling of urban flows.

A realistic --- yet relatively simple and computationally undemanding --- simulation of incompressible viscous flow through a random porous media has been demonstrated only recently in [1]. The crux of their approach is the representation of a solid phase by fictitious repelling body forces in the equations of motion, which rapidly attenuate flow to stagnation within the solid. The same approach to mimic the presence of solid structures and internal boundaries (cf. [8], for a review) was used in simulation of wind-tunnel flow past a scaled model of the Pentagon building [9]. Despite the different scales of porous-media grains and urban-media buildings, their solid geometry can be represented in the same manner, because the flows through both media are effectively governed by stiff elliptic boundary-value problem resulting from imposing the mass-continuity constraint on the flow. The analogy in the treatment of both media lead us address the influence of urban geometry and topology on the momentum flux in the atmospheric urban flow. The bulk volumetric properties of the urban canopy and estimated permeability are explored with the Navier-Stokes equations applied for the downtown areas of the Oklahoma City.

FLUID MODEL

The computational model EULAG employed in this study accommodates a broad class of flows and underlying fluid equations, in a variety of domains on scales from laboratory and wind tunnel, through terrestrial environments and climate, to stellar [10]. Furthermore, EULAG is formulated in generalized time-dependent curvilinear coordinates to facilitate grid adaptivity to targeted flow features and/or irregular evolutionary boundaries [11], and [12]. Here we integrate basic incompressible Navier-Stokes equations on a Cartesian domain, thus dispensing with many complexities of EULAG's analytic formalism. Focusing on buoyancy-driven flows of an anelastic fluid through an urban medium, the adopted Navier-Stokes equations can be compactly written as

$$\nabla(\bar{\rho}\cdot \mathrm{v}) = 0 \tag{1}$$

$$\frac{d\,\mathrm{v}}{dt} = -\nabla\pi' - g\frac{\theta'}{\bar{\theta}} + D_m(\kappa_m, e, \mathrm{v}) - \beta\,\mathrm{v} - \alpha_m\,\mathrm{v}' \tag{2}$$

$$\frac{d\theta'}{dt} = -\mathrm{v}\cdot\nabla\theta_e + D_h(\kappa_h, e, \theta) - \beta(\theta-\theta_B) - \alpha_h\theta' \tag{3}$$

$$\frac{de}{dt} = S(e) - \beta e \tag{4}$$

$$\frac{d\delta}{dt} = \mathrm{v} \tag{5}$$

where the prognostic variables include the three-dimensional velocity vector **v**, the potential temperature θ, the turbulent kinetic energy e, and a supplemental variable $\boldsymbol{\delta}$ representing the vector Eulerian field of Lagrangian displacements of fluid particles [1]. The overbears denote a reference state (i.e. $\bar{\pi}$, $\bar{\rho}$, $\bar{\theta}$; both $\bar{\rho}$, $\bar{\theta}$ are constant in current experiments, corresponding to the Boussinesq limit of the anelastic approximation); whereas, primes denote deviations from the geostrophically balanced ambient state, which may characterize external mesoscale flow conditions v_e, θ_e. The subscript B refers to the internal building state; e.g., $\mathrm{v}_B\equiv 0$, $\mathrm{e}_B\equiv 0$, θ_B. The mathematical operators appearing in the equations denote: the total time derivative $d/dt = \partial/\partial t + \mathrm{v}\cdot\nabla$; viscous dissipation of momentum via divergence of turbulent stress D_m and diffusion of heat D_h by the heat fluxes; sinks and source in the prognostic equation of the turbulent kinetic energy S. Furthermore, ρ denotes the density of air, π' is the normalized pressure perturbation from the ambient state, $\boldsymbol{g}=(0,0,-g)$ is the gravity vector, κ_m and κ_h are the eddy viscosity and diffusivity, respectively. The coefficients α_m and α_h are the reciprocals of (long) time scales of the Rayleigh friction and Newtonian cooling, the role of which is to attenuate the solution to prescribed ambient states in the vicinity of the open model boundaries. The coefficient β is the inverse time scale of the repelling body force introduced to mimic no-slip boundary conditions at the building walls. This variant of the immersed-boundary method (IMB) is particularly effective for simulating small scale transport and dispersion within intricate urban structures. Such an approximate imposition of internal-boundary conditions offers relative computational simplicity and massively-parallel efficacy, compared to schemes with explicit specification of the internal boundaries. The implicit time discretization of the repelling forces (i.e., a variant of the *feedback forcing* [13]) admits rapid attenuation of the flow to stagnation (within solid structures) in $O(\delta t)$ time comparable to the time step δt of the fluid model (see [9]; for an exposition). The governing equations (1)-(5) are integrated using the mesh-based (as oppose to particle based) non-oscillatory forward-in-time approach --- a signature of EULAG numerics, widely reviewed in the literature [10].

The EULAG-IMB modeling system has been applied through a range of scales, including simulation of Darcy flows in microscopic porous media [1], idealized flows around the complex isolated building structures [9] and realistic stratified atmospheric flows in large city environments: [14] and [15]. In the experiments discussed here, the ambient ambient conditions assume a neutrally stratified atmosphere and $\mathbf{v}_\mathrm{e}$=(3,0,0) m/s wind. The simulations discussed employ the grid consisting of 448^2 nodes in the horizontal, which covers the Central Business District (CBD) of Oklahoma City area together with its close outskirts, Figure 1, with uniform resolution $\Delta x=\Delta y$ = 4 m. In the vertical 51 grid points are used with grid interval Δz = 3 m, which suffices for the domain to extend above the highest

building. The building geometry is interpolated to the grid, from the GIS database.

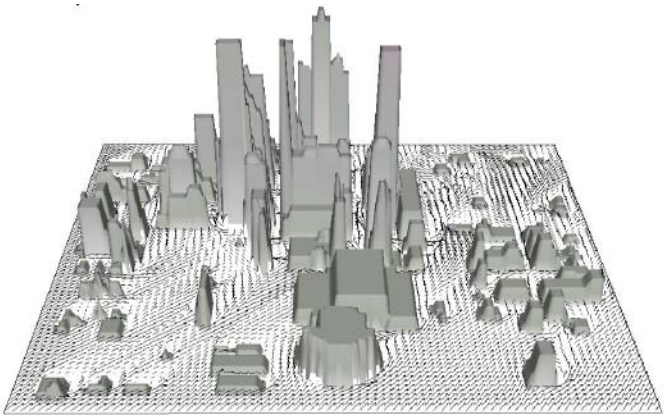

Figure 1. Structure of the Oklahoma City downtown embedded in EULAG simulations; arrows depict near surface wind.

Notably, the CBD modeled consists of the concentration of the tallest building structures present in the cities, with the largest density of contiguous building blocks and the highest surface roughness. It effects in significant differences in land surface characteristics in mesoscale modeling.

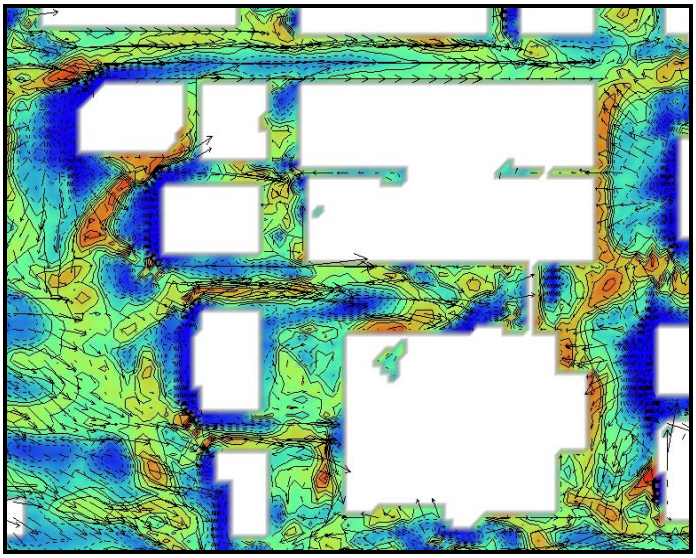

Figure 3. Horizontal cross-section of instantaneous vertical velocity and horizontal wind vectors at z=4 m above the ground.

Figure 3 highlights the simulated instantaneous flow, depicting vertical wind component and horizontal flow vectors at the height 4 m above the ground. It shows a highly complicated downtown flow that includes street canyon channeling effects and multi building interactions. Even at the scale of individual buildings, the turbulent flow structure is complicated due to sheared wind profile approaching the windward face of the building. This is illustrated in Figure 4, which shows the undisturbed incoming flow and two isolated buildings at an outskirt of the CBD. The wind decelerates along the mean wind direction and accelerates in the normal direction in order to pass over and around the building. Because of the shear an adverse pressure-gradient zone is created on the front wall of the building with a stagnant separation surface appearing at about two thirds of the building height. The wind above the stagnation surface flows upward and goes over the rooftop, while below the stagnation surface (the region seen at the plots at 4m above the ground) wind flows downward the building walls creating frontal eddy. When the downward flow reaches the ground level, a horse-shoe vortex is generated at the base of the buildings windward face, forcing air to flow downwind around the sides of the building. At the lee-ward side of the buildings the flow forms a highly turbulent cavity zone of negative pressure and reduced mean velocity.

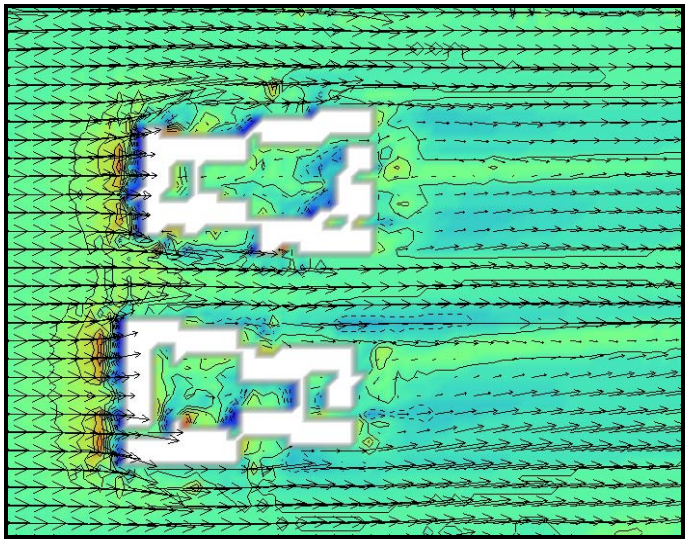

Figure 4. As in Figure 3, but for undisturbed inflow at an outskirt.

URBAN POROUS MEDIA

Here we present the analysis of UCL in terms of porous media analogy, with a lofty goal to parameterize morphological parameters of urban environments for the use in mesoscale numerical simulations. The UCL for Oklahoma City downtown, Figure 1, is viewed as a three-dimensional medium with background geostrophic conditions above the building roofs and local conditions below the UCL height distinct from the boundary layer flow outside urban areas.

The urban canopy described in terms of porous media consists of the void (pore) and the solid (grain) space. The former is composed of simply-connected streets, parks, parking lots as well as multiply-connected closed cavities (e.g. backyards, atriums); whereas the latter is represented by building volumes. Consequently, the traditional volumetric UCL information, such as building mean height and planar geometry, may be extended with the characteristics used to describe flows in porous media, such as porosity, grain-size distribution, permeability and tortuosity. Standardly, the porosity ϕ is defined as a fraction of

a medium volume (V) available for transport

$$\phi = \frac{V_{voids}}{V_{voids} + V_{solids}} \tag{6}$$

To accommodate vertical structure of UCL, we define porosity as the medium volume fraction (available for transport) per unit of the medium depth; that is, as the normalized building area at each level z of the model; whereupon $\phi(z)=0$ when there is no building at a z *level*, and $\phi(z)=1$ when entire urban area is occupied by buildings. Figure 5 shows the distribution of the voids and solids for the case at hand. The distribution is normalized by the UCL area, so the *pores=1* represent the entire model domain free of any obstacles at this level. The maximum of *grains* occurs near the ground, accounting for the total horizontal coverage of the building footprints.

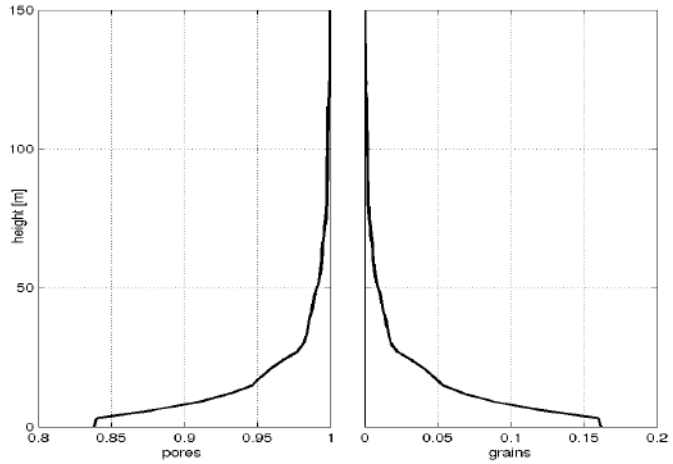

Figure 5. Normalized vertical distribution of pores and grains in UCL.

Figure 6 shows the corresponding pore-size frequency distribution at three selected elevations z = 0, 30, and 60 m. At the surface, the most frequent pore size is at the lower end of the spectrum, reflecting the intricacy of building structures. The secondary maximum evident at higher elevations reflects the concentration at large tall buildings in a relatively small area of UCL. Altogether, the figure documents the bimodality of UCL pore space consisting of large open areas around the CBD and of small voids between tall buildings within the CBD.

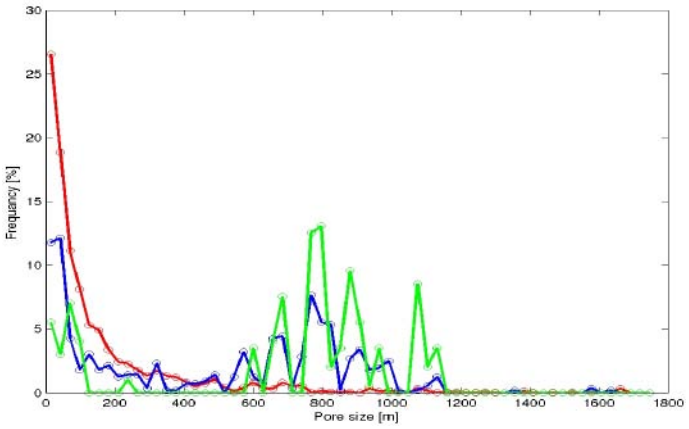

Figure 6. Pore size frequency distributions; red, blue and green lines correspond to z=0, 30 and 60 m elevations.

Another standard characteristic of porous media is the tortuosity T that quantifies an effective length of a path that fluid must travel in order to navigate through the media. A formal definition of the tortuosity (7) relates average length λ of flow trajectories passing through an arbitrary cross-section A in a time unit to the geometric length L of the media sample; here v

$$T = \frac{\int_A v(l)\lambda(l)dl \,/\, \int_A v(l)dl}{L} \tag{7}$$

is the velocity component in l direction. Because (7) is not easily computable with mesh-based methods, we employ a tortuosity measure instead, which consists of statistics of the Eulerain field of Lagrangian displacements $\delta(\mathbf{x}, t) = \mathbf{x}-\mathbf{x}_0$, with initial location of fluid particles $\mathbf{x}_0 = \mathbf{x}$**;** see [1] for a discussion.

INTEGRAL FLOW WITHIN URBAN CANOPY

Figure 7 shows the histories of the domain averaged total wind speed and of its vertical component. After the initial spin-up time $t_a=L/u_e \approx$ 600 sec, required for the ambient flow to pass the model domain, the averaged wind speed becomes essentially steady, with mean amplitude amplified compared to the ambient flow by the inverse of the total porosity factor (i.e. the volume of the open areas to the total volume of the domain).

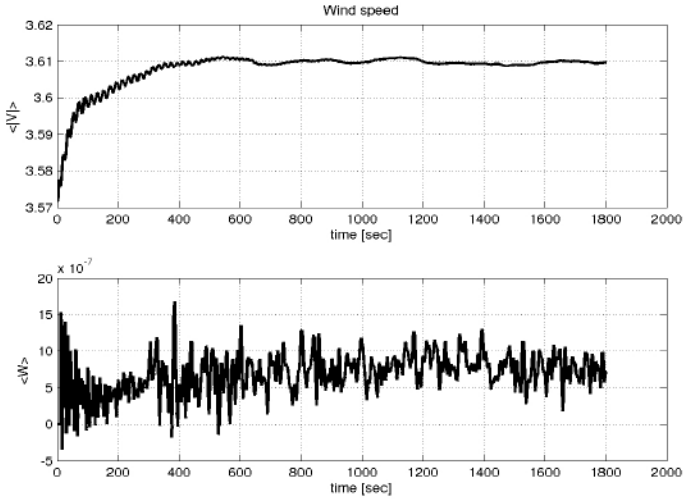

Figure 7. Time histories of the domain averaged wind speed |**v**| and vertical velocity <*w*>.

The domain averaged vertical velocity <w> ≈ $7*10^{-7}$ ms^{-1} is negligibly small compared to the mean flow, as implied by the mass continuity equation (1) with impermeable boundaries at

the top and the bottom of model domain. In essence, it evinces the assumed accuracy threshold [16] imposed in the solution of the elliptic pressure equation implied by (1).

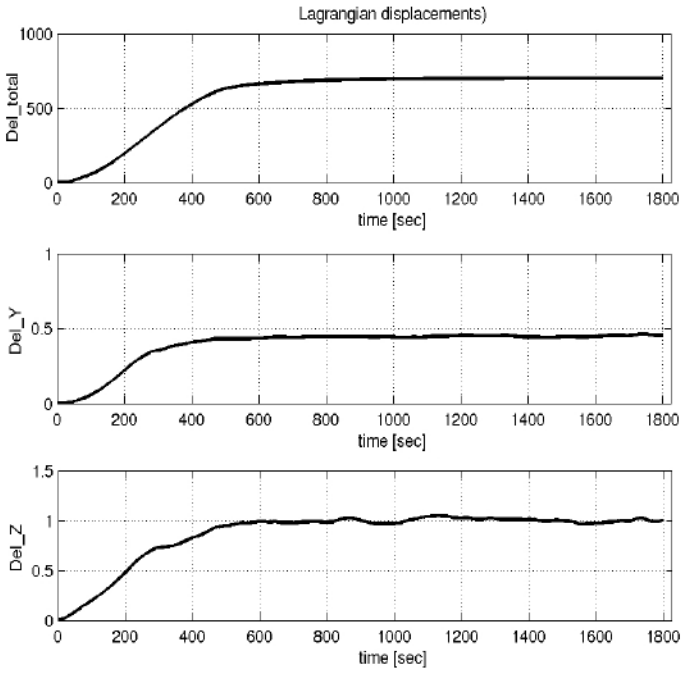

Figure 8. Histories of the L_2 norms of Lagrangian displacements: total (upper panel), crosswind (middle panel) and vertical (lower pannel).

Figure 8 presents histories of the domain averaged L_2 norms of Lagrangian displacements, normalized by the domain length in the respective directions. The total displacement (upper panel) is dominated by the ambient wind, while the mean fluctuating spanwise and vertical wind components are two orders of magnitudes smaller. This manifests that flow is predominantly in the x direction, and that a neutral atmospheric stability does not discriminate the vertical and horizontal air movements over and around the buildings. The factor of two between the vertical and spanwise displacements is intriguing; as it appears favor the vertical, while indicating the lack of equipartion of flow fluctuations in all three directions. Initially all the displacements grow linearly until the time t_a. After this initial stage the displacements in the vertical and in the spanwise tend to saturate with no significant changes in the time structure except with the small fluctuations of the vertical component, which can be attributed to a highly turbulent structure of the flow above the rooftops.

The time evolution of the horizontally averaged cross mean wind and vertical components of the Lagrangian displacements in function of model height is presented on Figure 9. After the initial 10 minute spin-up time, the vertical structure of these parameters is almost constant in time. The cross wind component shows the maximum displacement near the ground up to the approximate height ~50m, where the largest building density occurs. The vertical component shows more complicated structure with first weaker maximum near the ground, related to the turbulent structure of the frontal-eddies and leeward cavity zones. The second strongest layer above the 50m, represent the bulk effect of the upward air flow over the whole CBD area. In the mesoscale parameterizations of the UCL the along- and cross-mean wind frictional effects are usually accounted inside the surface layer models (SLM) based on the similarity theory, however the vertical flow disturbance is mostly omitted.

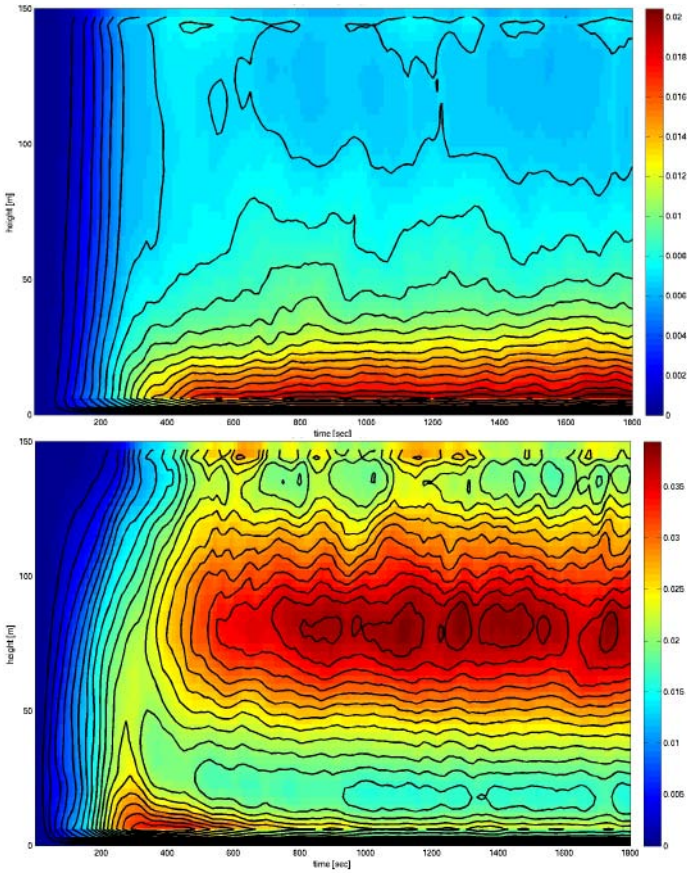

Figure 9. Time histories of the horizontally averaged Lagrangian displacements in the function of the model height. The lower and upper panels show, respectively, the crosswind and the vertical components and of the displacement.

In the low Reynolds number regime, the flow through classic porous media is governed by Darcy's law that links the fluid mass flux (discharge per unit area) F with the applied pressure gradient

$$F = -(\kappa / \mu) \cdot \nabla p \qquad (8)$$

where μ is the dynamic viscosity of the fluid, p is the measured pressure and κ is a proportionality constant known as permeability. Since the permeability is the property of the media

only, we first evaluate the characteristics of the fluid flow in the urban media by using the effective conductivity K=κ/μ factor.

$$K(z) \sim < -u'/(\rho^{-1}\partial p'/\partial x) >_{XY} \\ = < -u'/(\partial \pi'/\partial x) >_{XY} \quad (9)$$

Figure 10 shows the plot of the effective conductivity (9) in function of the model vertical coordinate. This effective conductivity is evaluated as a horizontal average of local conductivities based on local (mean at the level of LES model grid box) values of streamwise gradients of pressure perturbations and of streamwise velocity deviations from the undisturbed ambient flow.

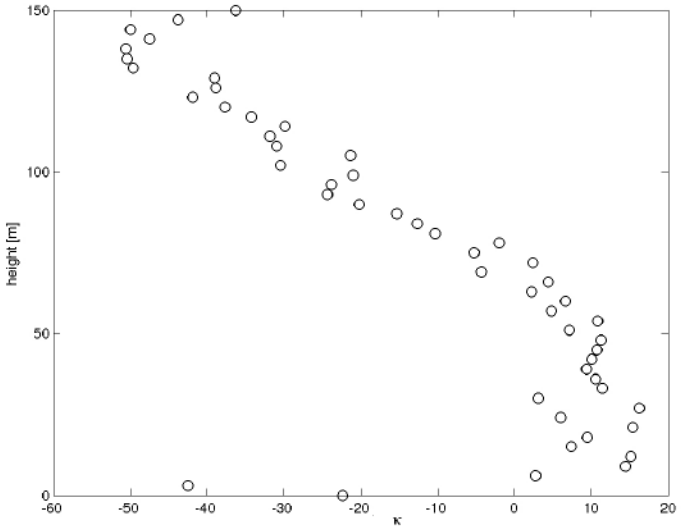

Figure 10. Effective conductivity in function of the model height.

Close to the ground the effective conductivity evinces negative values, thus indicating inapplicability of the porous media analogy there. However, above the shallow surface layer up to the 50 m height, which coincides with the extent of urban structures, it shows an approximately constant average value K=10 with the standard deviation $\sigma(K)\approx 2.5$. Aloft, $K(z)$ decreases linearly to take negative values at 70 m above the ground where the porosity approaches unity; cf. Fig. 5. The near ground negative values may be related to the coherent frontal eddies and lee-ward cavity zones where the reverse flows are correlated with respectively positive and negative pressure perturbations. Above the urban structures, the larger scale pressure gradients appear correlated with the acceleration of the flow in response to the obstacle effect of the entire urban area.

In order to represent properties of the media, rather than the properties of the flow through the media, (9) should account for the effective dynamic viscosity. In the large Reynolds flows inside the urban environment the dynamic viscosity may be determined by the eddy viscosity parameters computed within the model subgridscale parameterization. An adequate estimation of the permeability will be essential to relate the flow dynamics to corresponding media factors. In [1] it is shown that the media tortuosity growth with increasing pore size reveals distinct regimes of simulated flows, thus aiding interpretation of numerical results. To resolve low permeability flow near the model surface the model resolution may need to be increased, since the constant geometry of the buildings defines realistically small size of pores. Furthermore, the relation will need to be examined between permeability, porosity and torturosity, in terms of the classic porous media dependence

$$\kappa \sim \phi^3/(T^2A^2) \quad (10)$$

where A is the specific footprint of building structures [17].

URBAN POROUS MEDIA PARAMETERIZATION

The mesoscale models do not have the spatial resolution to properly simulate the fluid flow transport and turbulence at scales of the separate buildings and even on scales of larger urban structures. The urban effects in mesoscale models are incorporated using various approximate approaches [18-20]. The simplest approach in development Urban Canopy Parameterizations (UCP) is to modify the existing surface similarity theory schemes introducing morphological-based aerodynamic characteristics (as effective roughness lengths, displacement height, urban heating sources) in the form of urban LULC classes. The more sophisticated schemes accounts for urban effects in their turbulence closure scheme [21], or detailed urban canyon energy balance [22]. The next level of sophistication in UCP models implements multi-layers to account for effects of canyon streets, walls, and roofs based on three dimensional (3D) building morphology/geometry and detailed surface covers (e.g. trees) [23-24].

Representing the macroscopic properties of UCL (e.g. pressure and temperature gradients, drag effects) in the UCP is a complex task which requires to link properly the three-dimensional urban morphology and microstructure of the flow at the building and street level scales. Based on the results of our numerical experiments, we will examine next the usability of porous media analogy to construct the parameterization of the urban processes in the mesoscale models. The porous approach is usually adopted in vegetation canopy models to define parameterization of surface layer effects. In [25] the author uses the porous media analogy to compute urban mechanical effects of the horizontal flow orthogonal to street direction. In the continuation of this study we plan to use the static and dynamic characterization of the urban morphology in terms of porosity and tortuosity to test the permeability suitable for defining large-scale pressure gradients. The additional morphological features of the multi-level UCL that measure pore size distribution and their relative orientation against mean

flow trajectory can be estimated with simplified indicators of rugosity and sinuosity [26]. The rugosity factor accounts for the product of the height of urban canopy elements and their footprint area. The sinusoity factor defines the mean alignment of the elongated open elements to the mean flow direction. With higher sinuosity factor one can expect stronger resistance of the UCL to the mean flow. These structural parameters characterizing the geometrical complexity of the multi-layer urban media will be used to estimate distributed drag forces exerted by flow and the global effect of canopy obstacles on the slowing down of the mean wind speed within UCL. Aloft the UCL, the contributions from individual surface roughness elements are expected to blend into representative averages.

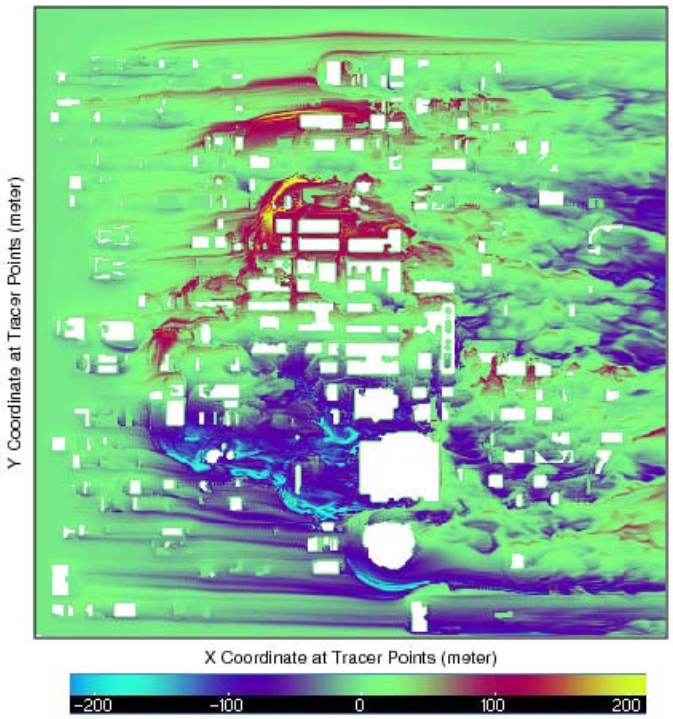

Figure 11. The cross wind component of the Lagrangian displacements seen at the height of 10 m above the ground.

While the urban canopy seen at the mesoscale model grid is usually represented by the homogeneous set of parameters, the majority of the real CBDs shows anisotropy of the medium morphology; e.g., the tortuosity is usually higher in the vertical than in the horizontal. In particular, because of the large aspect ratio of the height to the characteristic horizontal size of buildings in CBD areas, in the typical atmospheric conditions the flow tends around rather than over the buildings, as illustrated in Figure 4. Furthermore, Figure 11 shows the cross wind Lagrangin displacements near the ground. The air tends to flow not only around the single buildings but also it has strong cross mean wind components at the scale of the entire CBD area. Such an alteration of the mean wind speed due to small scale anisotropy of the canopy element sizes and the bulk anisotropy of CBD architectural structures calls for a systematic study. In future work we will extend accordingly the present analysis and evaluate the usability of the porous media analogy in the development of the mesoscale parameterizations.

ACKNOWLEDGMENTS

Computer time was provided by NSF MRI Grant CNS-0421498, NSF MRI Grant CNS-0420873, NSF MRI Grant CNS-0420985, NSF sponsorship of the National Center for Atmospheric Research, the University of Colorado, and a grant from the IBM Shared University Research (SUR) program.

REFERENCES

[1] Smolarkiewicz, *P.*, Winter, *C.* L., 2010. ”Pores resolving simulation of Darcy flows”. *Journal of Computational Physics*, **229**, doi: 10.1016/j.jcp.2009.12.031

[2] Ellefsen, R., 1990/1991. ”Mapping and measuring buildings in the canopy boundary layer in ten U.S. cities”. *Energy and Buildings*, **15-16**, 1025-1049.

[3] McPherson, T. N. and M. J. Brown, 2003. “Determination of the spatial and temporal distribution of population for air toxics exposure assessments”, *5th AMS Urban Env. Conf.*, Vancouver, B.C., 11 pp. LA-UR-04-4912.

[4] Cionco, R. M. and R. Ellefsen, 1998. “High resolution urban morphology data for urban wind flow modeling”. *Atm. Env.*, **32**(1), 7-17.

[5] Grimmond, C. S. B. and T. Oke, 1999. “Aerodynamic properties of urban areas derived from analysis of surface form”. *J. Appl. Met.*, **38**, 1262-1292.

[6] Burian, S.J., Brown, M.J., Augustus, N., 2007. “Development and assessment of the second generation National Building Statistics database”. *Seventh Symposium on the Urban Environment*, September, 10-13, 2007, San Diego, CA, USA.

[7] Ching, J., Brown, M., Burian, S., Chen, F., Cionco, R., Hanna, A., Hultgren, T., McPherson, T., Sailor, D., Taha, H., and Williams, D., 2009. "National urban database and access portal tool, NUDAPT". *Bulletin of the American Meteorological Society (BAMS)* doi: 10.1175/2009BAMS2675.1

[8] Mittal, R., and G. Iaccarino,2005. “Immersed Boundary Methods”. *Ann. Rev. Fluid Mech*. **37**, 239–261

[9] Smolarkiewicz, P.K., R. Sharman, J. Weil, S.G. Perry, D. Heist, and G Bowker, 2007. “Building resolving large-eddy simulations and comparison with wind tunnel experiments”. *J. Comput. Phys*., **227**, 633–653.

[10] Prusa, J.M., P.K. Smolarkiewicz and A.A Wyszogrodzki, 2008. “EULAG, a Computational Model for Multiscale Flows”. *Comput. Fluids*, **37**, 1193–1207.

[11] Wedi N.P., and P.K. Smolarkiewicz, 2004. “Extending Gal-Chen and Somerville terrainfollowing coordinate transformation on time dependent curvilinear boundaries”. *J. Comput. Phys*., **193**, 1–20.

[12] Smolarkiewicz P.K., and J.M. Prusa, 2005. "Towards mesh adaptivity for geophysical turbulence: continuous mapping approach". *Int. J. Numer. Meth. Fluids*, **47**, 789–801.

[13] Goldstein D., R. Handler, and L. Sirovich, 1993. Modeling a no-slip flow boundary with an external force field, *J. Comput. Phys*. **105**, 354–366.

[14] Wyszogrodzki A.A., and P.K. Smolarkiewicz, 2009. "Building resolving large-eddy simulations (LES) with EULAG".. *Academy Colloquium on Immersed Boundary Methods: Current Status and Future Research Directions*, 15-17 June 2009, Academy Building, Amsterdam, the Netherlands.

[15] Wyszogrodzki, A.A., F. Chen, S. G. Miao, and J. Michalakes, 2009. "Two-way coupling approach between WRF NWP and EULAG LES models for urban area transport and dispersion modeling". *Eighth Symposium on the Urban Environment*, 10-15 January 2009, Phoenix Arizona, USA

[16] Smolarkiewicz P.K, V. Grubiˇsi´c, L.G. Margolin 1997. "On forward-in-time differencing for fluids: stopping criteria for iterative solutions of anelastic pressure equations" Monthly Weather Rev. 125, 647–654.

[17] Matyka, M., Khalili, A. and Koza, Z., 2008. Tortuosity-porosity relation in porous media flow. *Physical Review E*, **78**, 026306-1--026306-8.

[18] Brown, M. J., 2000. "Urban parameterizations for mesoscale meteorological models. *Mesoscale Atmospheric Dispersion*". Ed., Z. Boybeyi., pp. 193-255.

[19] Bornstein, R. D. and K. J. Craig, 2002. "Survey of the history of the urbanization of numerical mesoscale models". Preprints, *Fourth Symposium on the Urban Environment*, 20-24 May, 2002, Norfolk, VA, USA

[20] Martilli, A., 2007. "An overview of advanced urbanization of mesoscale models". *Seventh Symposium on the Urban Environment,* September 10-13, 2007, San Diego, CA.

[21] Brown M. and M. Williams, 1998. "An urban canopy parameterization for mesoscale meteorological models", *2nd AMS Urban Environment Symposium*., November 2-6, 1998, Albuquerque, NM, USA. LA-UR-98-3831.

[22] Masson, V., 2000. "A physically-based scheme for the urban energy budget in atmospheric models". *Boundary-Layer Meteorol.* **98**, 357-397.

[23] Martilli, A., A. Clappier, and M.W. Rotach, 2002. "An urban surface exchange parameterization for mesoscale models". *Boundary-Layer Meteorol.* **104**, 261-304.

[24] Chen F., M. Tewari, K. Manning, S. Miao, A. Martilli, S. Grossman-Clarke, H. Kusaka, 2009. "Development of the ntegrated WRF/Urban modeling system and its application to urban environmental problems". Proceedings of the 7th *International Conference on Urban Climate*, 29 June - 3 July 2009, Yokohama, Japan

[25] Martilli, A. 2002. "Numerical study of urban impact on boundary layer structure: Sensitivity to wind speed, urban morphology, and rural soil moisture". *J. Appl. Meteor*., **41**, 1247–1266.

[26] Adolphe L. 2001. "A simplified model of urban morphology: application to an analysis of the environmental performance of cities". *Environment and Planning B*, **28**, 183-200.